Molecular Pharmacology Fast Forward. Published on November 12, 2013 as doi:10.1124/mol.113.089631
This article has not been copyedited and formatted. The final version may differ from this version.

Structural and Functional Analysis of G Protein-Coupled Receptor Kinase Inhibition by Paroxetine and a Rationally Designed Analog

Kristoff T. Homan, Emily Wu, Michael W. Wilson, Puja Singh, Scott D. Larsen, and John J. G. Tesmer

Life Sciences Institute and the Departments of Pharmacology and Biological Sciences, University of Michigan, Ann Arbor, Michigan 48109 (K.T.H, E.W., P.S., J.J.G.T.)

Vahlteich Medicinal Chemistry Core and the Department of Medicinal Chemistry, University of Michigan, Ann Arbor, Michigan 48109 (M.W.W., S.D.L.)

Molecular Pharmacology Fast Forward. Published on November 12, 2013 as DOI: 10.1124/mol.113.089631
This article has not been copyedited and formatted. The final version may differ from this version.

Running Title: **Inhibition of GRKs by Paroxetine Analogs**

Correspondence should be addressed to:

John J.G. Tesmer, Ph.D.
Life Sciences Institute
The University of Michigan
210 Washtenaw Ave. Rm 3425
Ann Arbor, MI 48109
Phone 734-615-9544
Fax 734-763-6492
Email: tesmerjj@umich.edu

Number of text pages:	29
Number of tables	3
Number of figures:	7
Number of references:	38
Number of words in abstract:	240
Number of words in introduction:	595
Number of words in discussion:	1652

List of Abbreviations:

ANS: anilinonaphthalene-8-sulfonic acid
bROS: bovine rod outer segments
CHAPS: 3-[(3-cholamidopropyl)dimethylammonio]-1-propanesulfonic acid
DDM: n-Dodecyl-β-D-Maltoside
DMSO: dimethyl sulfoxide
DTT: dithiothreitol
GPCR: G protein-coupled receptor
GRK: G Protein-coupled receptor kinase
MES: 4-morpholineethanesulfonic acid
PDB: protein data bank
PH: pleckstrin homology
P-loop: phosphate binding loop
PKA: protein kinase A
PKC: protein kinase C
P-loop: phosphate-binding loop
RGS: regulator of G protein signaling
RH: RGS homology
SSRI: selective serotonin reuptake inhibitor

Molecular Pharmacology Fast Forward. Published on November 12, 2013 as DOI: 10.1124/mol.113.089631
This article has not been copyedited and formatted. The final version may differ from this version.

Abstract

Recently we identified the serotonin reuptake inhibitor paroxetine as an inhibitor of G protein-coupled receptor kinase 2 (GRK2) that improves cardiac performance in live animals. Paroxetine exhibits up to 50-fold selectivity for GRK2 versus other GRKs. A better understanding of the molecular basis of this selectivity is important for the development of even more selective and potent small molecule therapeutics and chemical genetic probes. We first sought to understand the molecular mechanisms underlying paroxetine selectivity among GRKs. We directly measured the K_D for paroxetine and assessed its mechanism of inhibition for each of the GRK subfamilies, and then determined the atomic structure of its complex with GRK1, the most weakly inhibited GRK tested. Our results suggest that the selectivity of paroxetine for GRK2 largely reflects its lower affinity for adenine nucleotides. Thus, stabilization of off-pathway conformational states unique to GRK2 will likely be key for the development of even more selective inhibitors. Next, we designed a benzolactam derivative of paroxetine that has optimized interactions with the hinge of the GRK2 kinase domain. The crystal structure of this compound in complex with GRK2 confirmed the predicted interactions. Although the benzolactam derivative did not significantly alter potency of inhibition among GRKs, it exhibited 20-fold lower inhibition of serotonin reuptake. However, there was an associated increase in the potency for inhibition of other AGC kinases, suggesting that the unconventional hydrogen bond formed by the benzodioxole ring of paroxetine are better accommodated by GRKs.

Molecular Pharmacology Fast Forward. Published on November 12, 2013 as DOI: 10.1124/mol.113.089631
This article has not been copyedited and formatted. The final version may differ from this version.

Introduction

G protein-coupled receptor (GPCR) kinases (GRKs) initiate the termination of GPCR signaling via the phosphorylation of cytoplasmic loops and carboxy-terminal tails of activated GPCRs, which targets these receptors for deactivation through arrestin binding and clathrin-mediated endocytosis (Gurevich et al., 2012). Proper regulation of GPCRs by GRKs is critical for normal cellular signaling. For example, during heart failure GRK2 is overexpressed, which leads to the uncoupling of β adrenergic receptors (βARs) from normal sympathetic control (Ungerer et al., 1993; Ungerer et al., 1994). In fact, dominant negative inhibition of GRK2, achieved via adeno-associated virus administration of the C-terminal portion of GRK2 (βARKct), effectively restores a normal phenotype and βAR signaling in cellular and animal models of heart failure (Akhter et al., 1999; Raake et al., 2013; Rockman et al., 1998). Small molecule inhibitors of GRK2 would also serve as important clinical therapeutics as well as useful biochemical probes to understand GRK2 function in living cells (Shirakawa, 2009). Recently, we identified the selective serotonin reuptake inhibitor (SSRI) paroxetine, an FDA approved drug, as a relatively selective inhibitor of GRK2 (Thal et al., 2012). Paroxetine was reported to exhibit an IC_{50} of 20 μM and up to 50-fold selectivity over other GRKs such as GRK1 and GRK5, which represent the GRK1 and GRK4 subfamilies, respectively (Mushegian et al., 2012). Structural analysis of the GRK2·paroxetine complex indicated that the drug occupies the adenine, ribose, and polyphosphate binding subsites in the active site (Fig. 1A). The residues that paroxetine interacts with in the active site are highly conserved among GRKs, and thus the mechanism underlying its selectivity for GRK2 could not be divined from this structure alone. However, because paroxetine stabilizes the kinase domain of GRK2 in a conformation that has not been observed in other reported GRK2·inhibitor complexes (Tesmer et al., 2012; Thal et al., 2011), this structure could serve as a unique platform for the development of GRK2 selective inhibitors distinct from other classes currently known GRK2 inhibitors as well as from other protein kinase A, G and C (AGC kinase) family members.

With the long term goal of developing more selective inhibitors of GRK2, we sought to determine the molecular basis for the selectivity of paroxetine for GRK2 by directly determining the affinity of paroxetine for various GRKs, its inhibition constants

Molecular Pharmacology Fast Forward. Published on November 12, 2013 as DOI: 10.1124/mol.113.089631
This article has not been copyedited and formatted. The final version may differ from this version.

and mechanisms of inhibition for GRK1 and GRK2, and its atomic structure in complex with GRK1, the GRK most weakly inhibited by paroxetine. These results suggest that paroxetine traps the kinase domain of GRKs in a conformation similar to that used to bind ADP, and that the selectivity of paroxetine among GRKs is driven primarily by differences in their affinities for adenine nucleotides, in particular ADP. To probe the role of an unusual hydrogen bond formed by the benzodioxole ring of paroxetine in the GRK active site, we modeled and then synthesized a benzolactam derivative of paroxetine (CCG-206584) that would have optimized hydrogen bonds with the hinge region of GRK2 (Fig. 1B,C). This alteration did not lead to more potent inhibition of the GRKs, but did exhibit a 20-fold reduction in SSRI activity, confirming that kinase inhibition can readily be uncoupled from “off target” effects. We then solved the crystal structure of the GRK2·CCG-206584 complex, which confirmed our design principles. However, other AGC kinases exhibited an order of magnitude increased potency of inhibition relative to the parent compound. Thus, GRKs seem better suited to accommodate the benzodioxole ring of paroxetine than other AGC kinases. Together, these results provide important new insights into how paroxetine and its derivatives function as selective inhibitors of GRKs.

Materials and Methods

Protein purification. Rhodopsin in bovine rod outer segments (bROS) was prepared as previously reported (Papermaster, 1982). Bovine $GRK1_{1\text{-}535}$, bovine and human $GRK2_{S670A}$, bovine GRK5, and human palmitoylation deficient GRK6 (pal^-) were purified via a common procedure consisting of Ni-NTA affinity, Source15S, and tandem S200 size exclusion chromatography as previously described (Lodowski et al., 2006; Thal et al., 2012).

Bio-Layer Interferometry. GRKs were biotinylated with 400 μM EZ-Link HPDP-Biotin (ThermoScientific) for 2 h at room temperature or overnight at 4 ˚C prior to purification via tandem S-200 size exclusion chromatography to isolate only properly folded biotinylated protein. A Fortébio Octet RED system was used to measure the binding of small molecules to each GRK. Streptavidin coated tips were soaked for at least 15 min

Molecular Pharmacology Fast Forward. Published on November 12, 2013 as DOI: 10.1124/mol.113.089631
This article has not been copyedited and formatted. The final version may differ from this version.

to rehydrate the streptavidin prior to protein loading. Biotinylated GRKs (0.05 mg/ml) in assay buffer (20 mM HEPES pH 7.0, 5 mM $MgCl_2$, and 0.025% DDM) were then bound to the streptavidin tips for 30 min and washed in buffer for 10 min to remove any unbound kinase. DDM was included in order to help disrupt any potential small molecule aggregates, and the concentration used does not significantly inhibit GRK activity (data not shown). These conditions were designed to be similar to those used for kinetic assays. The protein loaded tips were then sequentially placed in a buffer supplemented with 1% DMSO for 1 min to reach a stable baseline, then in buffer supplemented with paroxetine and 1% DMSO for 3 min, and then placed back into the baseline buffer to allow dissociation to occur for 5 min. Changes in refractive index were analyzed with FortéBio's Data Analysis 7.0, and averaged reference sensor measurements were used for baseline subtraction prior to data processing. The association and dissociation curves were individually fit using GraphPadPrism using a two-phase model. The final k_{on} and k_{off} rate constants were constrained to be shared among all data sets for each individual GRK and used to calculate the ensemble dissociation constants (K_D=k_{off}/k_{on}).

Kinetic Assays. GRK kinetic assays were conducted in a buffer containing 20 mM HEPES pH 7.0, 2 mM $MgCl_2$, and 0.025% DDM with 50 nM GRK and 500 nM ROS in 5 min reactions. The low salt concentration and DDM were used to maximize GRK activity and disrupt small molecule aggregates from forming, respectively. For mechanism of inhibition by paroxetine with respect to ATP, the concentration of ATP was varied 1–100 μM and the concentration of paroxetine was varied 4–1000 μM. Reactions were quenched with SDS loading buffer, separated via SDS-PAGE, dried and exposed with a phosphorimaging screen prior to quantification via Typhoon imager, as previously reported (Thal et al., 2012). Data was analyzed and inhibition curves were fit via GraphPad Prism. The most appropriate model of inhibition was determined using the Akaike Information Criteria by comparing competitive and noncompetitive models of inhibition. PKC assays were conducted with the PKCα Kinase Enzyme System (Promega) in which 0.1 μg PKCα was added to 1 μg CREBtide substrate, PKC lipid activator, and 50 μM ATP for 30 min. After the initial reaction, ADP-Glo™ Reagent was

Molecular Pharmacology Fast Forward. Published on November 12, 2013 as DOI: 10.1124/mol.113.089631
This article has not been copyedited and formatted. The final version may differ from this version.

added to the reaction and allowed to incubate for an additional 40 min. Finally the Kinase Detection Reagent was added and allowed to incubate for 30 min and the luminescence was measured with a Pherastar imaging system. PKA assays were performed with the ADP-Glo system using 0.1 μg PKA and 1 μg Kemptide substrate, and 50 μM ATP for 30 min prior to addition of Kinase Detection Reagent and imaging on a Pherastar system.

Fluorescence Polarization Displacement Assay. Each kinase was first incubated with BODIPY TR-ADP (Invitrogen) in assay buffer (20 mM HEPES pH 8, 150 mM NaCl, 5 mM $MgCl_2$ and 2 mM DTT) for 10 min at room temperature in the dark. Note that higher ionic strength is used than in the Octet Red and kinetic assays, but as inhibitor binding is not expected to be strongly salt dependent, such should not prevent comparing relative effects among GRKs in each assay. The GRK-fluor mixture was then incubated with various concentrations of small molecule compounds in a 96-well plate (Corning, black plate). The plate was incubated at room temperature for an additional 10-15 min in the dark before measuring millipolarization on a Pherastar plate reader (excitation at 575 and emission at 620 nm). The concentration of kinase used during competition assays (3.5 μM bovine GRK1, 4 μM human GRK2, and 4 μM human GRK6 (Pal^-)) corresponds to the K_D estimated from equilibrium direct binding FP assays in which each GRK was titrated against a fixed concentration of BODIPY TR-ADP (25, 50, and 100 nM, respectively) wherein non-specific binding was determined by addition of 20 mM EDTA. GraphPad Prism was used to fit curves according to a one site competition with ligand depletion model wherein the K_D variable was shared between each individual experiment for each GRK.

GRK1·Paroxetine Crystal Structure Determination. Paroxetine (from a 10 mM stock dissolved in water) and $MgCl_2$ were added to a 7-8 mg/ml $bGRK1_{535}$ protein solution to attain a final concentration of 5 mM and 2 mM, respectively. Crystals were obtained via vapor diffusion using hanging drops consisting of 1.0 μl of protein and 1.0 μl of well solution, which consisted of 1 M NaCl, 100 mM MES pH 5.75, and 12-15% PEG3350. Crystals appeared in approximately 3 d and continued to grow in size for at least a

Molecular Pharmacology Fast Forward. Published on November 12, 2013 as DOI: 10.1124/mol.113.089631
This article has not been copyedited and formatted. The final version may differ from this version.

week. During harvesting, the crystals were cryoprotected by addition of 25% ethylene glycol to the drops prior to flash freezing in liquid nitrogen. Diffraction data was collected at the Advanced Photon Source (APS) on the LS-CAT beamline ID-G at a wavelength of 1.0793 Å. The diffraction data collected was anisotropic with the highest resolution reflections extending to 2.3 Å and 3.4 Å spacings in the highest and lowest resolution directions, respectively. As such, the data was subjected to an elliptical mask with major and minor axes corresponding to the highest resolution data limits (Lodowski et al., 2003). Indexing, integration, and scaling were performed with HKL2000 (Otwinowski and Minor, 1997). A molecular replacement solution was achieved with the Phaser module of CCP4 using PDB entry 3C50 as a search model (McCoy et al., 2007; Winn et al., 2011). Refinement was performed with the Refmac5 module of CCP4 and model building was conducted with Coot (Emsley and Cowtan, 2004; Murshudov et al., 1997). Differential crystal contacts involving each of the RH domains leads to conformational differences in the loops linking helices α6, α7, and α8. In chain A, the active site tether region is completely ordered due to unique lattice contacts, whereas the analogous region of chain B exhibits a similar degree of order as observed in other GRK1·ADP complexes (Singh et al., 2008). The final model was validated with MolProbity (Chen et al., 2010) prior to deposition of coordinates and structure factors in the PDB as entry 4L9I.

GRK2·CCG-206584–G$\beta\gamma$ Structure Determination. Human GRK2 and G$\beta\gamma$ were mixed in a 1:1 ratio and concentrated to a final total protein concentration of 4.5 mg/ml in the presence of 1 mM CCG-206584 (from a 50 mM stock in DMSO) and 2 mM $MgCl_2$. Crystals were obtained via the vapor diffusion method using hanging drops consisting of 0.8 μl protein solution added to an equal volume of well solution, which consisted of 1.2 M NaCl, 100 mM MES 7.0, and 9% PEG3350. Crystals appeared in approximately 4 d and continued to grow in size for several weeks. During harvesting the crystals were cryoprotected through the addition of 25% ethylene glycol to the harvested crystals prior to flash freezing in liquid N_2. Diffraction data was collected at APS on LS-CAT beamline ID-D at a wavelength of 1.1272 Å. The data collected was highly anisotropic with data extending to 2.4 Å and 3.5 Å spacings in the highest and lowest resolution directions,

Molecular Pharmacology Fast Forward. Published on November 12, 2013 as DOI: 10.1124/mol.113.089631
This article has not been copyedited and formatted. The final version may differ from this version.

respectively. The data was subjected to an elliptical mask with major and minor axes corresponding to the highest resolution data limits before scaling (Lodowski et al., 2003). Indexing, integration and scaling were performed with HKL2000 (Otwinowski and Minor, 1997). A molecular replacement solution was achieved with the Phaser module of CCP4 using PDB entry 3V5W as a search model (McCoy et al., 2007; Thal et al., 2012; Winn et al., 2011). Refinement was performed with the Refmac5 module of CCP4 and model building was conducted with Coot (Emsley and Cowtan, 2004; Murshudov et al., 1997; Winn et al., 2011). In the GRK2·CCG-206584 complex, there are several minor structural differences from the analogous GRK2·paroxetine complex, such as in the α5-α6 loop of the RGS homology (RH) domain and ordering of the β1-β2 hairpin loop in the pleckstrin homology (PH) domain, likely due to differences in crystal packing environments. The final model was verified with MolProbity (Chen et al., 2010) prior to deposition in the PDB as entry 4MK0.

Chemistry. Chemical names follow CAS nomenclature. Starting reagents and solvents were purchased from Fisher Chemical and (3S,4R)-tert-butyl 4-(4-fluorophenyl)-3-(hydroxymethyl)piperidine-1-carboxylate **(1)** was obtained from Astatech. 5-hydroxyisoindolin-1-one was purchased from Sphinx Chemical. All chemicals were used without purification. Reactions were monitored by TLC using pre-coated silica gel 60 F254 plates. Silica gel chromatography was performed with silica gel (220-240 mesh) obtained from Silicycle. NMR spectra were recorded on a Varian 400 MHz spectrometer. Chemical shifts are reported in δ (parts per million), by reference to the hydrogenated residues of deuterated solvent as internal standard $CDCL_3$: δ = 7.28 (^{1}H NMR). Mass spectra were recorded on a Micromass LCT time-of-flight instrument utilizing the electrospray ionization mode. The purity of the compounds was assessed via analytical reverse phase HPLC with a gradient of 10-90% acetonitrile:water over 6 min (C18 column, 3.5 µm, 4.6x100 mm, 254 nm detection).

(3S,4R)-tert-butyl 4-(4-fluorophenyl)-3-((tosyloxy)methyl)piperidine-1-carboxylate (2). *p*-Toluenesulfonyl chloride (0.03 g, 0.16 mmol) was added to a 0 °C solution of compound **1** (0.05 g, 0.16 mmol) in dry 1:1 THF/ pyridine (2 ml). The resulting mixture

Molecular Pharmacology Fast Forward. Published on November 12, 2013 as DOI: 10.1124/mol.113.089631
This article has not been copyedited and formatted. The final version may differ from this version.

was stirred for 40 min at 0 °C then for 2 h at room temperature. The starting material was consumed by TLC and HPLC. The mixture was concentrated on a rotary evaporator and dried under high vacuum for 1 h. The resulting brown oil was used without further purification.

(3S,4R)-tert-butyl 4-(4-fluorophenyl)-3-(((1-oxoisoindolin-5-yl)oxy)methyl)piperidine-1-carboxylate (3). Cesium carbonate (0.69 g, 2.1 mmol) was added to a room temperature solution of 5-hydroxyisoindolin-1-one (0.32 g, 2.11 mmol) in dry DMF (2 ml). The resulting mixture was stirred 30 min at room temperature before adding a solution containing compound **2** (0.33 g, 0.71 mmol) in DMF (2 ml). The resulting mixture was heated at 65 °C for 1 h then cooled to 50 °C and stirred overnight. The reaction mixture was then cooled to room temperature and extracted 2x with equal volumes of ether. The combined ether extracts were washed with 1 N NaOH (2x), saturated NaCl (1x) and dried ($MgSO_4$). After evaporation *in vacuo*, the crude oil was purified by flash chromatography (MeOH/ CH_2Cl_2 gradient). Obtained compound **3** (0.1 g, 0.23 mmol, 31.9% yield) was a yellow oil. HPLC purity: 92% (t_R = 7.4 min). ^{1}H NMR (400 MHz, Chloroform-d) δ 7.68 (d, *J* = 8.5 Hz, 1H), 7.23 (m, 1H), 7.12 (ddd, *J* = 8.0, 5.3, 2.3 Hz, 2H), 7.04 – 6.88 (m, 2H), 6.83 (dd, *J* = 8.4, 2.2 Hz, 1H), 6.73 (d, *J* = 2.1 Hz, 1H), 4.48 (m, 1H), 4.32 (s, 2H), 4.21 (m, 1H), 3.72 (dd, *J* = 9.4, 2.9 Hz, 1H), 3.57 (dd, *J* = 9.4, 6.6 Hz, 1H), 2.90 – 2.47 (m, 3H), 2.22 – 1.86 (m, 1H), 1.86 – 1.53 (m, 2H), 1.47 (s, 9H). ESI+MS m/z 385.1 ($M+H^+$- t-butyl).

5-(((3S,4R)-4-(4-fluorophenyl)piperidin-3-yl)methoxy)isoindolin-1-one hydrochloride (CCG-206584). 4 M HCl in dioxane (0.5 ml, 2 mmol) was slowly added to a solution of compound **3** (0.08 g, 0.182 mmol) in methylene chloride. The mixture was stirred 2 h at room temperature before concentrating. The residue was triturated in EtOAc and ether, and then filtered to obtain the HCl salt of 5-(((3S,4R)-4-(4-fluorophenyl)piperidin-3-yl)methoxy)isoindolin-1-one (0.04 g, 0.12 mmol, 68 % yield) as a white hygroscopic solid. HPLC purity: 100% (t_R = 4.4 min). ^{1}H NMR (400 MHz, DMSO-d6) δ 8.94 (s, 2H), 8.28 (s, 1H), 7.48 (d, *J* = 8.2 Hz, 1H), 7.36 – 7.03 (m, 3H), 7.03 –

Molecular Pharmacology Fast Forward. Published on November 12, 2013 as DOI: 10.1124/mol.113.089631
This article has not been copyedited and formatted. The final version may differ from this version.

6.73 (m, 2H), 4.22 (s, 2H), 3.78 – 3.57 (m, 2H), 3.57 – 3.40 (m, 1H), 3.36 (d, *J* = 12.4 Hz, 1H), 3.11 – 2.73 (m, 3H), 2.08 – 1.62 (m, 3H). ESI+MS m/z 341.1 ($M+H^+$).

Thermal Denaturation Studies. Thermal denaturation assays were conducted using a ThermoFluor plate reader as previously described in a buffer containing 20 mM HEPES pH 7.0, 5 mM $MgCl_2$, 2 mM DTT, and 1mM CHAPS with 0.2 mg/ml final concentration of GRK and 100 μM ANS (Thal et al., 2012). The CHAPS detergent was used as previously reported to reduce the presence of aggregates in the experiment.

Serotonin reuptake inhibition. HEK-293 cells stably transfected with the serotonin reuptake transporter were cultured in DMEM media supplemented with 10% FBS and 1% PenStrep. For each reaction, 10^5 cells were added to each well of a 100 mm 24 well plate that had been coated with 0.05 mg/ml poly-D-lysine. Serotonin transporters were blocked through a 1 h preincubation with compound, which was then washed 3x with a buffer containing 25 mM HEPES pH 7.4, 120 mM NaCl, 5 mM KCl, 1.2 mM $MgSO_4$, 1.3 mM $CaCl_2$, and 1.3 mM KH_2PO_4. Next, 100 nM total 5-hydroxytryptamine (20 nM [^{3}H]5HT) was added to the wells to initiate a 10 min reaction that was terminated by 3 washes of cold PBS prior to lysis of the cells will 1% SDS. Lysed cells were added to 5 ml of scintillation cocktail and tritium counts were recorded. Data was plotted and inhibition curves fit with GraphPad Prism.

Results

The most straightforward explanation for selective inhibition of GRK2 by paroxetine would be if the drug binds to GRK2 with greater affinity than to other GRKs. To investigate whether differences in the binding or dissociation kinetics of paroxetine contributes to differences in its IC_{50} values, we used bio-layer interferometry, wherein the GRK is immobilized on a waveguide and changes in refractive index are measured as a function of time after addition or dilution of a small molecule. The technique can determine rates of association (k_{on}), dissociation (k_{off}) and binding constants (e.g. $K_D=k_{off}/k_{on}$). The k_{on} and k_{off} rates of paroxetine for GRK1, GRK2, and GRK5, representing each of the three vertebrate GRK subfamilies (Mushegian et al., 2012),

Molecular Pharmacology Fast Forward. Published on November 12, 2013 as DOI: 10.1124/mol.113.089631
This article has not been copyedited and formatted. The final version may differ from this version.

were similar (Fig. 2A and B, Table 1), although ~2-fold higher affinity was measured for GRK2. Thus, the selectivity we observed in our kinetic assays is not entirely accounted for by preferential association of the drug with GRK2.

Next, we turned to enzymatic assays in which we measured GRK-mediated phosphorylation of light-activated bROS wherein the concentration of ATP was varied versus several paroxetine concentrations in order to determine the inhibition constants (K_i's) for GRK1 (Fig. 3A) and GRK2 (Fig. 3B), which are the most weakly and strongly inhibited GRKs we have tested, respectively (Table 1). A caveat in interpreting these assays is that they cannot be run under strict Michaelis-Menten conditions, and, because the reaction is bireactant, the resulting inhibition constants are approximations that also depend on the concentration of and K_M for rhodopsin, as well as changes in affinity for one substrate that occur upon binding the other. The estimated K_i value for GRK2 (3.5 μM) is 20-fold lower than for GRK1 (78 μM), similar to the 50-fold difference measured for their IC_{50} values (Table 1). Surprisingly, the inhibition data for GRK1 and GRK2 was best fit by different models. Namely, the mechanism of paroxetine inhibition was noncompetitive for GRK1 (R^2 = 0.75, >99.9% probability according to the Akaike Information Criteria) and competitive for GRK2 (R^2 = 0.71, >99.9% probability) with respect to ATP.

Considered along with the bio-layer interferometry data, these results suggest that differences in affinities of these GRKs for competing substrates or products may be chiefly responsible for selectivity observed in enzymatic assays. We therefore determined the K_D of the ATP analog adenosine 5′-(β,γ-imido)triphosphate (AMPPNP) and ADP, representing the pre- and post-hydrolysis states of the phosphotransfer reaction, using a fluorescence polarization assay in which we monitored the displacement of BODIPY-TR ADP from the enzyme (Fig. 2C, Table 1). GRK2 exhibited a ~2-fold higher K_D for AMPPNP than GRK1 (106 vs. 49 μM), but a 30-fold higher K_D for ADP than GRK1 (46 versus 1.4 μM). Thus, during the catalytic cycle GRK2 retains ADP much less efficiently than GRK1, and thus is more susceptible to inhibition by paroxetine during catalysis. Interestingly, balanol exhibits ~10-fold selectivity for GRK2 based on IC_{50} values (Tesmer et al., 2010), and has 5-6 fold higher affinity for GRK2 as measured in the BODIPY-TR ADP displacement assay (Table 1). Thus, the selectivity

Molecular Pharmacology Fast Forward. Published on November 12, 2013 as DOI: 10.1124/mol.113.089631
This article has not been copyedited and formatted. The final version may differ from this version.

exhibited for GRK2 by compounds chemically unrelated to paroxetine is not necessarily as strongly dependent on the relative affinity of GRKs for ADP.

Next, we determined the crystal structure of GRK1 in complex with paroxetine using diffraction data extending to 2.3 Å spacings in the highest resolution direction (Table 2). The complex forms an asymmetric dimer in the asymmetric unit of the crystals using the same regulator of G protein signaling homology (RH) domain-mediated two-fold interface as observed in all prior structures of wild-type GRK1. The two GRK1 molecules exhibit a Cα RMSD (492 atomic pairs) of 0.69 Å for the entire molecule, and 0.47 Å (323 atomic pairs) when just the kinase domain structures are compared. Strong electron density for paroxetine is observed in the active sites of each kinase domain (Fig. 4A, B) in a conformation essentially identical to that of paroxetine bound to GRK2. In both chains, the kinase domain adopts a partially closed conformation that most closely resembles those of GRK1 in complex with ADP such as in PDB entries 3C50 (Singh et al., 2008), 3C4Z (Singh et al., 2008), and 3QC9 (Huang et al., 2011) (Z-scores of 25.4, 25.2, and 20.0, respectively, using the PDBeFold server (Krissinel and Henrick, 2004)). The kinase domains of 3C50 and 3C4Z exhibit a Cα RMSD of 0.64 Å RMSD (322 atomic pairs) and 0.65 Å (326 atomic pairs), respectively, versus chain A of the paroxetine complex. The kinase domain in the GRK1·paroxetine complex is, however, in a slightly different conformation, and a 3˚ rotation of the large lobe relative to the small lobe is required to achieve the best alignment with the ADP complexes. Interestingly, the GRK2 kinase domain in complex with paroxetine (Thal et al., 2012) is also more similar to that of GRK1·ADP (2.3 Å RMSD; 435 atomic pairs) than to those of other reported GRK2 structures. Thus, paroxetine seems to stabilize GRKs in a conformation similar to their ADP-bound state. Unfortunately, the structure of a GRK2·ADP complex is not currently available to confirm this prediction.

Several structural differences are evident upon comparison of the structures of GRK1 and GRK2 in complex with paroxetine (Fig. 4C). A 5˚ rotation of the large lobe of GRK2 relative to the small lobe is required to attain the same degree of closure of the kinase domain in the GRK1·paroxetine complex. In GRK2, there are hydrophobic interactions formed between paroxetine and the active site tether (AST) loop, but the GRK1 AST forms no direct contacts with the drug. The piperidine ring of paroxetine

Molecular Pharmacology Fast Forward. Published on November 12, 2013 as DOI: 10.1124/mol.113.089631
This article has not been copyedited and formatted. The final version may differ from this version.

seems better ordered in the GRK1 structure, and its nitrogen forms hydrogen bonds with the side chain of Asp271 and the backbone oxygen of Glu318. In GRK2, the piperidine nitrogen forms a hydrogen bond to a water molecule and to GRK2-Ala321 (analogous to GRK1-Glu318). This difference likely results from the slightly different conformation of these kinase domains. The phosphate binding loops (P-loops) in the structures of the GRK1·paroxetine and GRK2·paroxetine complexes also adopt distinct conformations, with atoms within the P-loop of the GRK2·paroxetine up to 0.9 Å closer to the bound drug than in the GRK1·paroxetine structure (Fig. 4C and 7B). However, neither conformation is more collapsed than the analogous loop in the GRK1·ADP complex, likely a consequence of its interactions with the diphosphate moiety of the nucleotide (Fig. 4C). Despite these differences, the buried accessible surface area of paroxetine in the GRK1 and GRK2 structures are nearly identical: 280 $Å^2$ and 270 $Å^2$, respectively, consistent with our observations that paroxetine exhibits similar K_D values towards each enzyme.

In the crystal structure of the GRK2·paroxetine–G$\beta\gamma$ complex (Thal et al., 2012), one of the most striking interactions between GRK2 and paroxetine are two specific hydrogen bonds formed between the backbone atoms of residues in the hinge of the kinase domain and an oxygen and a carbon in the small molecule (Fig. 1A). Carbon-oxygen hydrogen bonds are unusual and have lower free energy than conventional hydrogen bonds (Horowitz and Trievel, 2012). Therefore, substitution of the benzodioxole ring with a similar sized aromatic system, such as a benzolactam, might yield a more potent inhibitor due to the formation of two strong hydrogen bond with the hinge. The benzolactam derivative of paroxetine (CCG-206584) was synthesized in a straightforward three-step synthesis from commercially available alcohol **1** embodying both of the requisite stereocenters (Scheme 1). Tosylation of the alcohol and base-catalyzed displacement of the resulting tosylate **2** with 5-hydroxyisoindolin-1-one provided N-Boc benzolactam **3**. Cleavage of the Boc group under acidic conditions then afforded the HCl salt of the desired analog (Fig 1C).

To evaluate if CCG-206584 was capable of interacting with GRKs in a manner similar to that of paroxetine, we first measured its ability to thermostabilize GRKs from each of the three vertebrate subfamilies. CCG-206584 caused small but statistically

Molecular Pharmacology Fast Forward. Published on November 12, 2013 as DOI: 10.1124/mol.113.089631
This article has not been copyedited and formatted. The final version may differ from this version.

significant increases in the melting points of GRK1 and GRK5 relative to paroxetine (Fig. 5A): (2.3 ˚C for GRK1, 0.8 ˚C for GRK2, and 0.8 ˚C for GRK5), consistent with the formation of improved hydrogen bonds. We next evaluated the potency of inhibition by CCG-206584 for GRK1, GRK2, and GRK5 using two substrates: bROS and the soluble substrate tubulin (Fig. 5B and 5C). There were no significant changes in the affinity of CCG-206584 relative to paroxetine for any of the GRKs. We also tested the potency of inhibition against protein kinase A (PKA) and C (PKC), representing the broader AGC kinase family. Paroxetine was determined to have IC_{50} values of 45 and 220 μM, and CCG-206584 to have IC_{50} values of 2.6 and 26 μM for PKA and PKC, respectively (Fig. 6A). Thus, the introduction of conventional hydrogen bonds in CCG-206584 increased potency of inhibition of other AGC kinase family members and decreased selectivity for GRKs.

Development of the paroxetine scaffold into a kinase inhibitor must also coincide with reducing the “off-target” effect of serotonin reuptake inhibition. Previous studies have probed the structure-activity relationship of derivatives of SSRIs such as paroxetine (Marcusson et al., 1992; Mathis et al., 1992; Mathis et al., 1994), but a benzolactam derivative of paroxetine has not been reported. To assess how the alterations made to the paroxetine scaffold in CCG-206584 change the SSRI function of paroxetine, HEK-293 cells stably transfected with the serotonin transporter were used to compare the inhibition of serotonin reuptake by paroxetine and CCG-206584 (Fig. 6B). CCG-206584 was ~20-fold less able to inhibit serotonin uptake (IC_{50} = 38 ± 8 nM) compared to paroxetine (IC_{50} = 2 ± 0.3 nM), demonstrating that SSRI activity can readily be uncoupled from GRK inhibition.

To confirm our rational design approach, we also determined the crystal structure of the GRK2·CCG-206584–Gβγ complex (Fig. 7). Despite a different space group and unique crystal packing relative to the structure of the GRK2·paroxetine–Gβγ complex, the overall conformation of each structure is quite similar with an all atom RMSD for kinase domains of 0.79 Å (606 residues aligned using the PDBeFold Server). Comparison of paroxetine (bound to either GRK1 or GRK2) and CCG-206584 in the active site illustrate a highly conserved configuration (Fig. 7B). There is a small internal rotation between the two small molecules that results in the atoms of the benzolactam

Molecular Pharmacology Fast Forward. Published on November 12, 2013 as DOI: 10.1124/mol.113.089631
This article has not been copyedited and formatted. The final version may differ from this version.

ring of CCG-206584 shifting by up to 0.5 Å, which likely results from the formation of hydrogen bonds between CCG-206584 and the backbone of GRK2-Asp272 and Met274 (Fig. 7A and B). These bonds have distances of 2.8 Å and 2.7 Å, respectively, instead of 2.9 Å and 3.4 Å for their equivalents in the paroxetine complex. The backbone carbonyl of GRK2-Met274 also seems to rotate in order to avoid a steric clash with the benzolactam carbonyl. The hydrogen bond formed between the piperidine ring of each inhibitor and the backbone of GRK2-Ala321 is also maintained in both structures.

Discussion

The development of small molecule inhibitors for protein kinases has been of longstanding interest due to the regulatory roles played by these enzymes in signaling networks. However, to date there have been relatively few clinically useful kinase inhibitors beyond blockbuster receptor tyrosine kinase inhibitors such as imatinib (Nagar et al., 2002) or iressa (Yun et al., 2007). Several GRKs have also emerged as targets for the development of small molecule inhibitors, which would ultimately serve to increase the sensitivity of GPCRs to extracellular signals. Potent AGC kinase inhibitors known to be effective against GRKs include the natural products staurosporine (Ward and O'Brian, 1992), sangivamycin (Loomis and Bell, 1988), and balanol (Tesmer et al., 2010). However, the utility of these compounds is limited by their lack of selectivity and/or toxicity. Even more recently identified compounds synthesized by Takeda Pharmaceuticals, which exhibit selective inhibition of GRK2 over other GRKs (Thal et al., 2011) and AGC family kinases, have not progressed towards clinically relevant treatments (Ikeda et al., 2007).

Recently we identified the SSRI paroxetine as an inhibitor of GRK2 that exhibits 50-fold selectivity over other GRKs (Thal et al., 2012). Paroxetine was shown to effectively penetrate into cells, where it inhibits GRK2-dependent phosphorylation of an activated GPCR with an IC_{50} of ~35 μM, simulates increased contraction in isolated mouse cardiomyocytes, and generates more powerful contraction of the heart without associated changes in heart rate in live animals (Thal et al., 2012). A better understanding of the origins of paroxetine's selectivity for GRK2 would assist in the

Molecular Pharmacology Fast Forward. Published on November 12, 2013 as DOI: 10.1124/mol.113.089631
This article has not been copyedited and formatted. The final version may differ from this version.

design of improved, more selective chemical probes based on the paroxetine scaffold, itself being a successful FDA-approved drug since 1992. A common explanation for selectivity is differences in binding or dissociation kinetics due to distinct interactions with the target protein. However, bio-layer interferometry experiments showed that paroxetine binds to GRK1, GRK2 and GRK5 similarly with ~10 μM affinity, although highest affinity was for GRK2 (Fig. 2A, B; Table 1). Although unexpected, this result is consistent with paroxetine binding in the active site of the kinase domain where sequence and structural identity among GRKs is very high. We therefore hypothesized that the ~50-fold selectivity for GRK2 based on IC_{50} values is due to differences in the ability of the various GRKs to bind their nucleotide substrates and/or products, which would compete for the same site as paroxetine. Kinetic analysis of GRK1, the most weakly inhibited GRK, and GRK2, the most strongly inhibited, revealed that the two enzymes exhibit a 20-fold (78 μM vs 3.5 μM, respectively) difference in their K_i values, ~5-fold lower than their respective IC_{50} values. As expected for an inhibitor that binds in the active site, paroxetine exhibits a competitive mode of inhibition for GRK2 versus ATP (Fig. 3B). However, paroxetine inhibition of GRK1 is best fit with a noncompetitive model with respect to ATP (Fig. 3A). A noncompetitive mode of inhibition for a drug that binds in the active site is not without precedent in the AGC kinase family of enzymes. For example, staurosporine acts as a non-competitive inhibitor of PKC (Ward and O'Brian, 1992) even though crystal structures of the drug in complex with PKC (Xu et al., 2004) or PKA (Prade et al., 1997) demonstrate that the staurosporine binding site overlaps with that of ATP. The difference in mode of GRK inhibition may reflect different rate limiting steps in these GRKs, or that assumptions made in deriving Michaelis-Menten parameters are not fully valid, as necessitated by the assay conditions used for GRKs.

To further support the hypothesis that differential affinities of GRK1 and GRK2 for ATP and/or ADP may be responsible for the observed selectivity of paroxetine, we monitored the ability of the non-hydrolyzable ATP analog AMPPNP and the product ADP to displace a fluorescently labeled ADP ligand and showed that GRK2 has 2-fold higher K_D for AMPPNP and 30-fold higher K_D for ADP over GRK1 (Table 1, Fig. 2C). Therefore at steady state, paroxetine has to compete with more tightly bound ATP

Molecular Pharmacology Fast Forward. Published on November 12, 2013 as DOI: 10.1124/mol.113.089631
This article has not been copyedited and formatted. The final version may differ from this version.

and/or ADP in the case of GRK1. This observation is consistent with the fact that, despite the use of saturating conditions, we have not yet crystallographically resolved adenine nucleotides in the active site of GRK2, whereas GRK1 and GRK6 readily co-crystallize in complex with adenine nucleotides. The binding of rhodopsin to GRK1 is reported to increase the affinity of ATP binding (Pulvermuller et al., 1993). Therefore, during the catalytic cycle, preferential interaction of rhodopsin with GRK1 (K_M = 4 μM; V_{max} = 700 nmol/min/mg (Palczewski et al., 1988)), which represents a physiological pair, rather than with GRK2 (K_M = 6 μM; V_{max} = 72 nmol/min/mg (Benovic et al., 1987)) may also render it more difficult for ligands such as paroxetine to inhibit activity. However, this does not seem to be the case for the inhibitor balanol, which exhibits consistent IC_{50} versus K_D values among the GRKs tested (Table 1).

The crystal structure of the GRK1·paroxetine complex is generally consistent with the above conclusions. The orientation of the large and small lobes of the kinase domain of the GRK1·paroxetine complex is most similar to those exhibited by ADP bound complexes of GRK1. The conformation of the kinase domain in the GRK2·paroxetine–Gβγ complex is also more similar to those of the GRK1·ADP complexes than it is to any other reported GRK structure. Thus, the binding of paroxetine seems to drive the kinase domain of GRKs into a conformational state similar to that used to bind the product ADP, the ligand for which GRK1 and GRK2 exhibit the greatest difference in affinity (Table 1). Despite several differences in specific contacts with the drug, the total buried surface area for paroxetine is quite similar in GRK1 and GRK2, consistent with their similar k_{on} and k_{off} values measured by Octet Red (Fig. 2A,B).

Our analysis also provides new insight into the molecular basis for highly selective inhibition (>1000 fold) of GRK2 by the compounds produced by Takeda Pharmaceuticals Inc. (Thal et al., 2011). These molecules stabilize GRK2 in a conformation that is not expected to be along the normal GRK2 reaction coordinate. Such may account, at least in part, for the enhanced selectivity of these compounds. Notably, an RNA aptamer highly selective for GRK2 also trapped the kinase domain of GRK2 in a conformational state that is likely unique to the GRK2 subfamily of GRKs (Tesmer et al., 2012). Thus, achieving more selective inhibition of GRK2 may require

Molecular Pharmacology Fast Forward. Published on November 12, 2013 as DOI: 10.1124/mol.113.089631
This article has not been copyedited and formatted. The final version may differ from this version.

the development of paroxetine analogs that induce more “off-pathway” conformational states.

We hypothesized that the benzodioxole ring of paroxetine and its relatively weak interactions with the hinge of the kinase domain, an element that helps dictate the relative orientation of the large and small lobes, may be an important driver of selectivity. By substitution of a benzolactam, we predicted that we would introduce two strong hydrogen bonds between the small molecule and the hinge region of GRK2 without disrupting the overall configuration of the kinase domain. However, CCG-206584 yielded only subtle increases in thermostability for GRK1, GRK2 and GRK5, and no significant increase in potency. Thus, incorporation of a conventional hydrogen bond in place of the carbon-oxygen hydrogen bond did not yield a better GRK inhibitor. Instead, the potency of inhibition of PKA and PKC was increased about 10-fold (Fig. 6A). However, we confirmed a 20-fold decrease in potency of serotonin reuptake inhibition for CCG-206584 versus paroxetine (Fig. 6B). Thus, it is possible to select against SSRI activity, an “off target” effect, while retaining potency of GRK2 inhibition.

Using X-ray crystallography, we showed that the overall conformation of the GRK2 kinase domain is similar upon binding either inhibitor (Fig. 7A, B), and that both compounds bind in similar configurations in the active site. Furthermore, the chemical environment occupied by paroxetine in complex with GRK1 or GRK2 is highly conserved with that occupied by CCG-206584 (Fig. 7B). The strong electron density present in the omit maps of CCG-206584 (Fig. 7A) suggests that this compound is better ordered in the active site of GRK2 relative to paroxetine, although comparison of distinct crystal forms at different resolution limits is not straightforward. As predicted by rational design, the benzolactam group of CCG-206584 forms two conventional hydrogen bonds with the hinge while maintaining all the other interactions formed by paroxetine. However, as noted above, increased potency was only observed for inhibition of PKA and PKC. When the GRK2·balanol (Tesmer et al., 2010) and GRK2·CCG-206584–G$\beta\gamma$ structures are compared, it is observed that the *p*-hydroxybenzamide hydroxyl of balanol (Fig. 7C) makes similar hydrogen bonds to the hinge. Thus, introduction of the benzolactam ring may have conferred CCG-206584 with properties common to other pan-AGC kinase inhibitors such as balanol. After all,

Molecular Pharmacology Fast Forward. Published on November 12, 2013 as DOI: 10.1124/mol.113.089631
This article has not been copyedited and formatted. The final version may differ from this version.

analogous hydrogen bonds to the same hinge residues are also formed by the substrate ATP. We conjecture that kinases such as PKA and PKC have enough flexibility in their hinge region to accommodate the hydrogen bonds afforded by CCG-206584 while optimizing other contacts with the molecule, but are much worse than GRKs at accommodating the unconventional hydrogen bond afforded by the benzodioxole ring of paroxetine. Given that the binding of paroxetine and CCG-206584 to GRK2 results in a very similar overall conformation of the kinase domain, their similar potencies may reflect the fact that for GRKs the free energy for the formation and/or accommodation of optimized hydrogen bonds is not offset by the desolvation penalty for the more polar benzolactam group. In future analogs, a benzodioxole ring may be preferable to a benzolactam, at least if GRK selectivity is the only consideration.

In conclusion, our studies support the hypothesis that more potent and selective chemical probes with less off-target effects based on the paroxetine scaffold can be generated via structure-based drug design by exploiting structural/conformational features unique to GRK2. These molecules will serve as important tools to study GRK2 function in living cells and animals, and, potentially, as therapeutic leads for the treatment of cardiovascular disease.

Molecular Pharmacology Fast Forward. Published on November 12, 2013 as DOI: 10.1124/mol.113.089631
This article has not been copyedited and formatted. The final version may differ from this version.

Acknowledgments

We thank Drs. Peggy Gnegy and Bipasha Guptaroy for their expertise in setting up the serotonin reuptake experiments.

Molecular Pharmacology Fast Forward. Published on November 12, 2013 as DOI: 10.1124/mol.113.089631
This article has not been copyedited and formatted. The final version may differ from this version.

Authorship Contributions

Participated in research design: Homan, Larsen, and Tesmer.

Conducted experiments: Homan, Wu, and Singh

Chemical synthesis: Wilson

Performed data analysis: Homan and Singh

Wrote or contributed to writing of the manuscript: Homan, Larsen, and Tesmer.

References

Akhter SA, Eckhart AD, Rockman HA, Shotwell K, Lefkowitz RJ and Koch WJ (1999) In vivo inhibition of elevated myocardial β-adrenergic receptor kinase activity in hybrid transgenic mice restores normal β-adrenergic signaling and function. *Circulation* **100**(6): 648-653.

Benovic JL, Mayor F, Jr., Staniszewski C, Lefkowitz RJ and Caron MG (1987) Purification and characterization of the β-adrenergic receptor kinase. *J Biol Chem* **262**(19): 9026-9032.

Chen VB, Arendall WB, Headd JJ, Keedy DA, Immormino RM, Kapral GJ, Murray LW, Richardson JS and Richardson DC (2010) MolProbity: all-atom structure validation for macromolecular crystallography. *Acta Crystallogr D* **66**: 12-21.

Emsley P and Cowtan K (2004) Coot: model-building tools for molecular graphics. *Acta Crystallogr D Biol Crystallogr* **60**(Pt 12 Pt 1): 2126-2132.

Gurevich EV, Tesmer JJ, Mushegian A and Gurevich VV (2012) G protein-coupled receptor kinases: more than just kinases and not only for GPCRs. *Pharmacol Ther* **133**(1): 40-69.

Horowitz S and Trievel RC (2012) Carbon-oxygen hydrogen bonding in biological structure and function. *J Biol Chem* **287**(50): 41576-41582.

Huang CC, Orban T, Jastrzebska B, Palczewski K and Tesmer JJ (2011) Activation of G protein-coupled receptor kinase 1 involves interactions between its N-terminal region and its kinase domain. *Biochemistry* **50**(11): 1940-1949.

Ikeda S, Keneko M and Fujiwara S (2007) Cardiotonic agent comprising GRK inhibitor, (Ltd. TPC ed).

Krissinel E and Henrick K (2004) Secondary-structure matching (SSM), a new tool for fast protein structure alignment in three dimensions. *Acta Crystallogr D Biol Crystallogr* **60**(Pt 12 Pt 1): 2256-2268.

Lodowski DT, Pitcher JA, Capel WD, Lefkowitz RJ and Tesmer JJ (2003) Keeping G proteins at bay: a complex between G protein-coupled receptor kinase 2 and Gβγ. *Science* **300**(5623): 1256-1262.

Lodowski DT, Tesmer VM, Benovic JL and Tesmer JJ (2006) The structure of G protein-coupled receptor kinase (GRK)-6 defines a second lineage of GRKs. *J Biol Chem* **281**(24): 16785-16793.

Loomis CR and Bell RM (1988) Sangivamycin, a nucleoside analogue, is a potent inhibitor of protein kinase C. *J Biol Chem* **263**(4): 1682-1692.

Marcusson JO, Norinder U, Hogberg T and Ross SB (1992) Inhibition of [3H]paroxetine binding by various serotonin uptake inhibitors: structure-activity relationships. *Eur J Pharmacol* **215**(2-3): 191-198.

Mathis CA, Gerdes JM, Enas JD, Whitney JM, Taylor SE, Zhang Y, McKenna DJ, Havlik S and Peroutka SJ (1992) Binding potency of paroxetine analogues for the 5-hydroxytryptamine uptake complex. *J Pharm Pharmacol* **44**(10): 801-805.

Mathis CA, Taylor SE, Enas JD and Akgun E (1994) Binding potency of 6-nitroquipazine analogues for the 5-hydroxytryptamine reuptake complex. *J Pharm Pharmacol* **46**(9): 751-754.

McCoy AJ, Grosse-Kunstleve RW, Adams PD, Winn MD, Storoni LC and Read RJ (2007) Phaser crystallographic software. *J Appl Crystallogr* **40**(Pt 4): 658-674.

Murshudov GN, Vagin AA and Dodson EJ (1997) Refinement of macromolecular structures by the maximum-likelihood method. *Acta Crystallogr D* **53**: 240-255.

Mushegian A, Gurevich VV and Gurevich EV (2012) The origin and evolution of G protein-coupled receptor kinases. *PLoS One* **7**(3): e33806.

Nagar B, Bornmann WG, Pellicena P, Schindler T, Veach DR, Miller WT, Clarkson B and Kuriyan J (2002) Crystal structures of the kinase domain of c-Abl in complex with the small molecule inhibitors PD173955 and imatinib (STI-571). *Cancer Res* **62**(15): 4236-4243.

Otwinowski Z and Minor W (1997) Processing of X-ray diffraction data collected in oscillation mode. *Method Enzymol* **276**: 307-326.

Palczewski K, McDowell JH and Hargrave PA (1988) Purification and characterization of rhodopsin kinase. *J Biol Chem* **263**(28): 14067-14073.

Papermaster DS (1982) Preparation of retinal rod outer segments. *Methods Enzymol* **81**: 48-52.

Prade L, Engh RA, Girod A, Kinzel V, Huber R and Bossemeyer D (1997) Staurosporine-induced conformational changes of cAMP-dependent protein kinase catalytic subunit explain inhibitory potential. *Structure* **5**(12): 1627-1637.

Pulvermuller A, Palczewski K and Hofmann KP (1993) Interaction between photoactivated rhodopsin and its kinase: stability and kinetics of complex formation. *Biochemistry* **32**(51): 14082-14088.

Raake PW, Schlegel P, Ksienzyk J, Reinkober J, Barthelmes J, Schinkel S, Pleger S, Mier W, Haberkorn U, Koch WJ, Katus HA, Most P and Muller OJ (2013) AAV6.βARKct cardiac gene therapy ameliorates cardiac function and normalizes the catecholaminergic axis in a clinically relevant large animal heart failure model. *Eur Heart J* **34**(19): 1437-1447.

Rockman HA, Choi DJ, Akhter SA, Jaber M, Giros B, Lefkowitz RJ, Caron MG and Koch WJ (1998) Control of myocardial contractile function by the level of β-adrenergic receptor kinase 1 in gene-targeted mice. *J Biol Chem* **273**(29): 18180-18184.

Shirakawa T (2009) Clinical Trial Design for Adenoviral Gene Therapy Products. *Drug News Perspect* **22**(3): 140-145.

Singh P, Wang B, Maeda T, Palczewski K and Tesmer JJ (2008) Structures of rhodopsin kinase in different ligand states reveal key elements involved in G protein-coupled receptor kinase activation. *J Biol Chem* **283**(20): 14053-14062.

Tesmer JJ, Tesmer VM, Lodowski DT, Steinhagen H and Huber J (2010) Structure of human G protein-coupled receptor kinase 2 in complex with the kinase inhibitor balanol. *J Med Chem* **53**(4): 1867-1870.

Tesmer VM, Lennarz S, Mayer G and Tesmer JJ (2012) Molecular mechanism for inhibition of g protein-coupled receptor kinase 2 by a selective RNA aptamer. *Structure* **20**(8): 1300-1309.

Thal DM, Homan KT, Chen J, Wu EK, Hinkle PM, Huang ZM, Chuprun JK, Song J, Gao E, Cheung JY, Sklar LA, Koch WJ and Tesmer JJ (2012) Paroxetine is a direct inhibitor of G protein-coupled receptor kinase 2 and increases myocardial contractility. *ACS Chem Biol* **7**(11): 1830-1839.

Thal DM, Yeow RY, Schoenau C, Huber J and Tesmer JJ (2011) Molecular mechanism of selectivity among G protein-coupled receptor kinase 2 inhibitors. *Mol Pharmacol* **80**(2): 294-303.

Ungerer M, Bohm M, Elce JS, Erdmann E and Lohse MJ (1993) Altered expression of β-adrenergic receptor kinase and β_1-adrenergic receptors in the failing human heart. *Circulation* **87**(2): 454-463.

Ungerer M, Parruti G, Bohm M, Puzicha M, DeBlasi A, Erdmann E and Lohse MJ (1994) Expression of β-arrestins and β-adrenergic receptor kinases in the failing human heart. *Circ Res* **74**(2): 206-213.

Ward NE and O'Brian CA (1992) Kinetic analysis of protein kinase C inhibition by staurosporine: evidence that inhibition entails inhibitor binding at a conserved region of the catalytic domain but not competition with substrates. *Mol Pharmacol* **41**(2): 387-392.

Winn MD, Ballard CC, Cowtan KD, Dodson EJ, Emsley P, Evans PR, Keegan RM, Krissinel EB, Leslie AGW, McCoy A, McNicholas SJ, Murshudov GN, Pannu NS, Potterton EA, Powell HR, Read RJ, Vagin A and Wilson KS (2011) Overview of the CCP4 suite and current developments. *Acta Crystallogr D* **67**: 235-242.

Xu ZB, Chaudhary D, Olland S, Wolfrom S, Czerwinski R, Malakian K, Lin L, Stahl ML, Joseph-McCarthy D, Benander C, Fitz L, Greco R, Somers WS and Mosyak L (2004) Catalytic domain crystal structure of protein kinase C-θ (PKCθ). *J Biol Chem* **279**(48): 50401-50409.

Yun CH, Boggon TJ, Li Y, Woo MS, Greulich H, Meyerson M and Eck MJ (2007) Structures of lung cancer-derived EGFR mutants and inhibitor complexes: mechanism of activation and insights into differential inhibitor sensitivity. *Cancer Cell* **11**(3): 217-227.

Footnotes

This work was supported by the National Institute of Health grants [HL071818 & HL086865] to J.J.G.T. and the American Heart Association grant [N014938] to K.T.H. Use of the Advanced Photon Source was supported by the U. S. Department of Energy, Office of Science, Office of Basic Energy Sciences, under Contract No. DE-AC02-06CH11357, and use of LS-CAT Sector 21 was supported by the Michigan Economic Development Corporation and Michigan Technology Tri-Corridor Grant [085P1000817].

Molecular Pharmacology Fast Forward. Published on November 12, 2013 as DOI: 10.1124/mol.113.089631
This article has not been copyedited and formatted. The final version may differ from this version.

Legends for Schemes

Scheme 1. Synthesis of CCG-206584. (a) TsCl, THF, pyr; (b) 5-hydroxyisoindolin-1-one, Cs_2CO_3; (c) HCl, dioxane.

Molecular Pharmacology Fast Forward. Published on November 12, 2013 as DOI: 10.1124/mol.113.089631
This article has not been copyedited and formatted. The final version may differ from this version.

Legends for Figures

Figure 1: Structure of paroxetine bound to GRK2 and of inhibitors used in this study. A) Paroxetine in the active site of GRK2 in the GRK2·paroxetine–Gβγ complex (PDB entry 3V5W). The kinase domain large lobe is colored yellow and the small lobe green. Paroxetine is drawn as a stick model with carbons colored cyan, oxygens red, and nitrogens blue. Three hydrogen bonds, including an unconventional C-O hydrogen bond, are shown black dashed lines with associated distances. Chemical structures of paroxetine (B) and its benzolactam derivative CCG-206584 (C).

Figure 2. Quantitative measurement of ligand binding to GRKs. Rates of paroxetine association (A) and dissociation (B) using GRKs representing each GRK subfamily (GRK1, GRK2, and GRK5), as measured by bio-layer interferometry on an Octet RED. Both sets were best fit by a biphasic model that was interpreted to be comprised of both specific and non-specific interactions between paroxetine and the protein. Only the specific portions of k_{on} (1600 ± 120, 1200 ± 110, and 1100 ± 62 $M^{-1}s^{-1}$ for GRK1, GRK2 and GRK5, respectively) and k_{off} (0.021 ± 0.0003, 0.008 ± 0.0002, and 0.015 ± 0.0002 s^{-1} for GRK1, GRK2, and GRK5, respectively) were used to calculate K_D values (13, 7.3, and 14 μM, respectively). Error bars represent the SEM for 3 independent experiments performed in duplicate. C, Fluorescence polarization competition binding experiments revealed a 30-fold higher affinity binding of ADP to GRK1 (1.4 μM) versus GRK2 (46 μM). Error bars represent SEM for 2 independent experiments performed in triplicate.

Figure 3. Inhibition kinetic assays with GRK1 and GRK2. Paroxetine was determined to inhibit GRK1 (A) non-competitively (>99% likelihood) with a K_i of 78 μM versus ATP, whereas GRK2 (B) is inhibited competitively (>99% likelihood) with a K_i of 3.5 μM vs. ATP. Error bars represent SEM for 3 independent experiments performed in duplicate.

Figure 4. Structural analysis of the GRK1·paroxetine complex. A) Overview of the complex. Paroxetine binds to GRK1 in the active site at the interface of the small and large lobes of kinase domain (light blue). The RH domain (darker blue) is shown for

reference. An omit map calculated at 3 σ (green mesh) is shown for paroxetine (stick model with carbons colored yellow, nitrogens blue and fluorines teal) within the active site. B) Detailed view of paroxetine within the GRK1 active site. Hydrogen bonds formed by paroxetine (black dashed lines terminating in grey spheres) that range from 2.8 Å to 3.2 Å are formed with main chain atoms in the hinge (Thr265 and Met267) and the large lobe (backbone of Glu318 and side chain of Asp271). C) The conformation of the kinase domain in the structure of the GRK1·paroxetine complex (light blue) strongly resembles its conformation in the GRK2·paroxetine (PDB entry 3V5W, green) and GRK1·ADP (PDB entry 3C4Z, wheat) complexes. The AST loop of Chain A in the GRK1·paroxetine complex is more distant from the drug than in GRK2 complex and forms no direct contacts, and its P-loop is displaced furthest from the ligand binding site relative to the other two structures. For example, there is a 2.3 Å displacement of the Cα atom of Gly196 in the P-loop between the ADP and paroxetine complexes of GRK1, likely due to engagement of the P-loop by the polyphosphate tail of ADP in the GRK1·ADP structure. Atoms in the P-loop of the GRK1·paroxetine structure are displaced by up to 0.9 Å away from the drug relative to the GRK2·paroxetine structure. ADP from the 3C4Z structure (stick model with carbons colored wheat) is shown for reference. Both ADP and paroxetine form analogous hydrogen bonds with backbone atoms of Thr265 and Met267 in the hinge of the GRK1 kinase domain.

Figure 5: CCG-206584 selectivity and potency for GRKs. A) CCG-206584 (CCG) thermostabilizes GRKs to a greater extent than paroxetine (pax). The melting temperature (T_m) was determined from the inflection point of sigmoidal curves fit to thermal denaturation data. Data shown is collected from 4 experiments performed in triplicate with error bars showing SEM. Significant increases in the thermal stabilization of CCG-206584 relative to paroxetine were observed for GRK1 ($P<0.0001$) and GRK5 ($P=0.016$). (B) Inhibition of representative members of the three GRK subfamilies (GRK1, GRK2 and GRK5) in response to CCG-206584 using the soluble substrate tubulin. Data shown is representative of at least 4 experiments performed in duplicate and the error bars represent standard deviation in the experiment shown. (C) Analogous assays using light-activated rhodopsin in rod outer segments as the substrate. Data

Molecular Pharmacology Fast Forward. Published on November 12, 2013 as DOI: 10.1124/mol.113.089631
This article has not been copyedited and formatted. The final version may differ from this version.

shown is representative of at least 3 experiments performed in duplicate and the error bars represent standard deviation of the experiment shown.

Figure 6: Comparison of the potency of paroxetine and CCG-206584 for non-GRK targets. A) CCG-206584 (CCG) is ~20x and ~10x more potent inhibitor of PKA and PKC, respectively, relative to paroxetine (pax). Data shown is representative of 5 experiments for PKA and 3 experiments for PKC, performed in duplicate. The error bars represent standard deviation. B) CCG-206584 inhibits serotonin uptake by HEK-293 cells stably expressing the serotonin transporter approximately 20-fold less potently than paroxetine. The data is representative of 5 experiments performed in triplicate with error bars showing standard deviation of the experiment.

Figure 7: Crystallographic analysis of the GRK2·CCG-206584 complex. A) Electron density F_o-F_c omit map contoured at 3σ (green mesh) of CCG-206584 bound to the active site of GRK2 (gray cartoon). The compound makes specific hydrogen bonds to backbone atoms of Asp272, Met274 and Ala321, shown as black dashed lines, B) Superposition of the active sites of the GRK2·paroxetine–Gβγ, GRK2·CCG-206584–Gβγ, and GRK1·paroxetine complexes based on alignment of their small lobes. The small and large lobes of the kinase domain in the GRK2·paroxetine complex are colored green and yellow, respectively, and the carbons of paroxetine are colored cyan. The GRK1 complex is colored blue with blue carbons in paroxetine. All molecules bind in a similar conformation in the active site. The rationally designed CCG-206584 undergoes a small rotation towards the hinge region of GRK2 that allows it to form 2.7 Å and 2.8 Å hydrogen bonds with Asp272 and Met274, respectively. C) Superposition of the GRK2·balanol complex (PDB entry 3KRW) with that of GRK2·CCG-206584–Gβγ by pair fitting key Cα residues in the active site (GRK2 residues 201, 272, 273, 274, and 321). GRK2 in complex with balanol is drawn in the color wheat. Despite distinct relative conformations adopted by the large and small lobes of each kinase, both CCG-206584 (dark gray carbons) and balanol (pink carbons) form analogous hydrogen bonds (balanol green and CCG-206584 dark green) to backbone atoms in the hinge.

Molecular Pharmacology Fast Forward. Published on November 12, 2013 as DOI: 10.1124/mol.113.089631
This article has not been copyedited and formatted. The final version may differ from this version.

TABLE 1

Interaction of small molecules with GRKs

	GRK1 (μM)	GRK2 (μM)	GRK5 (μM)	GRK6 (μM)
$K_{D\ (paroxetine)}$	13	7.3	14	N.D.
$K_{i\ (paroxetine)}$ (vs. ATP)	78 ± 10	3.5 ± 0.9	N.D.	N.D.
$K_{M\ (ATP)}$	3.2 ± 0.5	8.8 ± 0.5	N.D.	N.D.
$K_{D\ (ADP)}$ (FP)	1.4 ± 0.2	46 ± 16	N.D.	11 ± 2
$K_{D\ (AMPPNP)}$ (FP)	49 ± 15	110 ± 20	N.D.	190 ± 7
$K_{D\ (balanol)}$ (FP)	0.55 ± 0.2	0.074 ± 0.07	N.D.	0.30 ± 0.15
$IC_{50\ (balanol)}$ [a]	0.34	0.042	0.16	0.49

Values represent mean ± SEM. N.D., not determined; FP, measured by fluorescence polarization (this study). [a] from Tesmer et al. 2010.

Molecular Pharmacology Fast Forward. Published on November 12, 2013 as DOI: 10.1124/mol.113.089631
This article has not been copyedited and formatted. The final version may differ from this version.

TABLE 2

Crystallographic statistics

Protein complex	GRK2·CCG-206584–Gβγ	GRK1·paroxetine
X-ray source	LS-CAT ID-D	LS-CAT ID-G
Wavelength (Å)	1.1272	1.0793
D_{min}(Å)	19.99-2.4 (2.44-2.4)	29.9-2.32 (2.36-2.32)
Space group	$C222_1$	$P\,2_12_12_1$
Cell constants	a=61.2, b=240.9, c=212.0	a=66. 8, b=122.1, c=152.9
Unique reflections	30794	54845
R_{sym} (%)	10.6 (39.0)	10.9 (94.9)
Completeness (%)	49.9 (1.0)	36.9 (0.8)
$\langle I\rangle/\langle\sigma_I\rangle$	61.7/4.0 (7.0/3.0)	49.7/1.8 (5.4/2.0)
Redundancy	5.0 (2.8)	9.1 (9.2)
Refinement resolution (Å)	20.0-2.4 (2.47-2.4)	29.9-2.32 (2.38-2.32)
Total reflections used	29079	51966
RMSD bond lengths (Å)	0.004	0.009
RMSD bond angles (°)	0.875	1.4
Est. coordinate error (Å)	0.409	0.30
Ramachandran plot		
most favored, outliers (%)	94.1, 0.1	96.7, 0.1
R_{work}	19.5 (38.3)	18.8 (24.5)
R_{free}	24.6 (81.1)	22.9 (28.8)
Protein atoms	8235	7894
Water molecules	147	309
Inhibitor atoms	25	48
Average B-factor (Å^2):	55.3	23.4
Protein	55.9	19.4
Inhibitor	50	20.8
MolProbity score	1.28 (100th percentile)	1.37 (100th percentile)
MolProbity Ramachandran outlier	1	1
MolProbity Cβ deviations	0	0
MolProbity bad backbone bonds	0	0
MolProbity bad backbone angles	0	0
PDB Entry	4MK0	4L9I

* Low completeness values reflect the fact that an elliptical mask was applied prior to scaling was used to accommodate highly anisotropic diffraction data (Lodowski et al., 2003). Without the mask, data had 82.4% overall completeness and 82% in the highest resolution shell for 4MK0 and 100% overall completeness and 100% completeness in the highest resolution shell for 4L9I.

Molecular Pharmacology Fast Forward. Published on November 12, 2013 as DOI: 10.1124/mol.113.089631
This article has not been copyedited and formatted. The final version may differ from this version.

TABLE 3

Inhibition of GRK phosphorylation of tubulin and rhodopsin by paroxetine and CCG-206584

		paroxetine		CCG-206584	
		$plogIC_{50}$ ± SEM	n	$plogIC_{50}$ ± SEM	n
Tubulin	GRK1	3.8 ± 0.04	7	3.8 ± 0.06	5
	GRK2	5.6 ± 0.04	9	5.6 ± 0.03	7
	GRK5	3.9 ± 0.05	4	4.0 ± 0.06	6
Rhodopsin	GRK1	3.5 ± 0.07 [a]		3.7 ± 0.4	3
	GRK2	4.7 ± 0.04 [a]		5.2 ± 0.04	5
	GRK5	3.6 ± 0.03 [a]		4.1 ± 0.07	4

[a] from Thal et al 2012. Errors represent the SEM from n experiments performed in duplicate.

Molecular Pharmacology Fast Forward. Published on November 12, 2013 as DOI: 10.1124/mol.113.089631
This article has not been copyedited and formatted. The final version may differ from this version.

Scheme 1

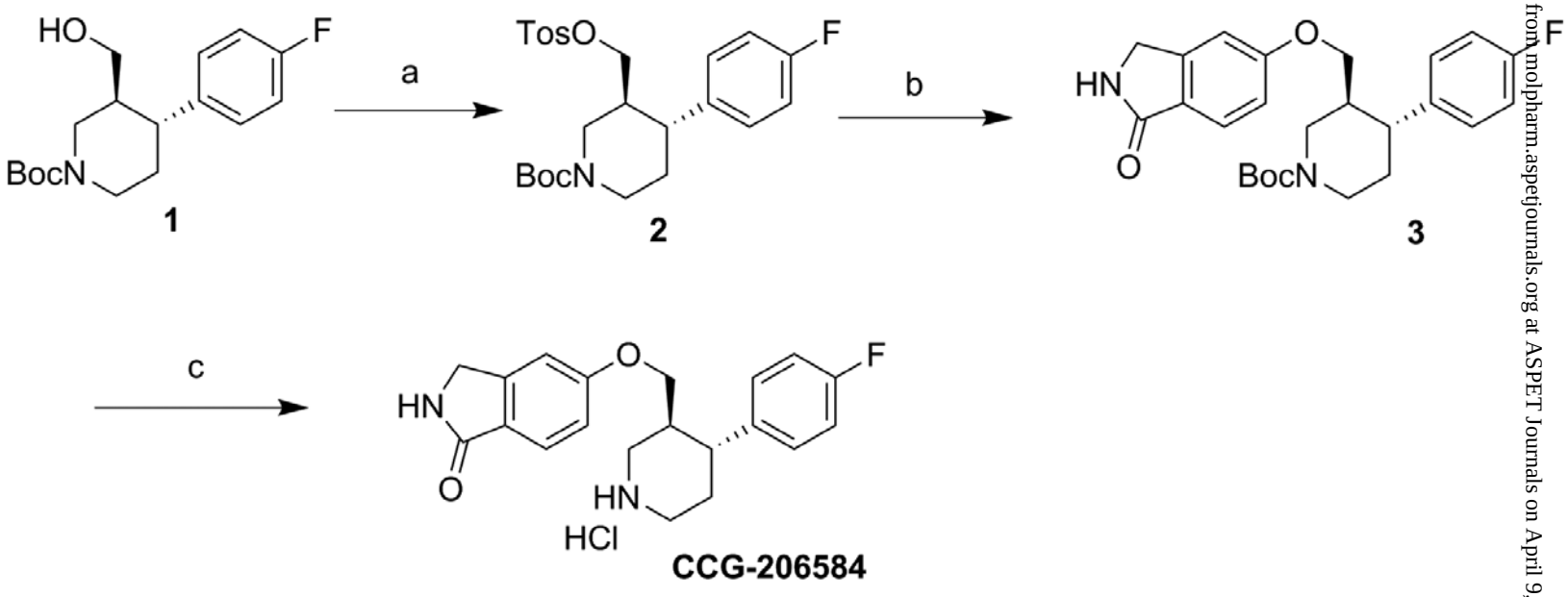

1 2 3 CCG-206584

Molecular Pharmacology Fast Forward. Published on November 12, 2013 as DOI: 10.1124/mol.113.089631
This article has not been copyedited and formatted. The final version may differ from this version.

Figure 1

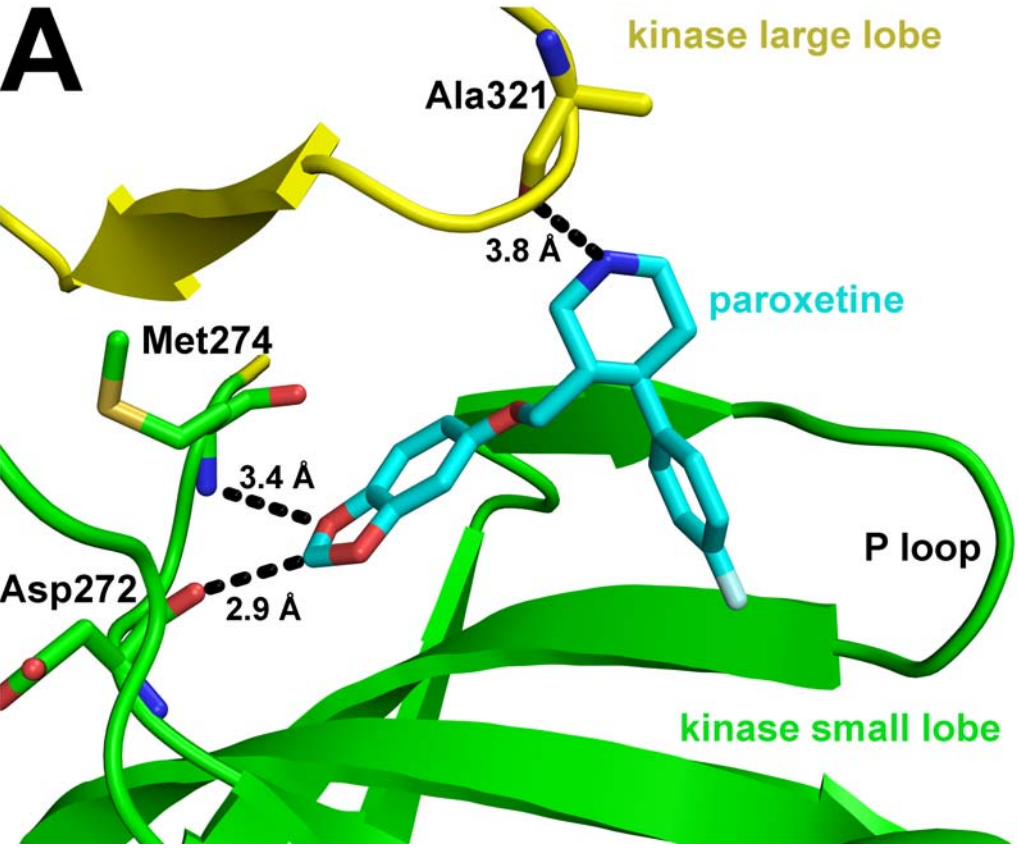

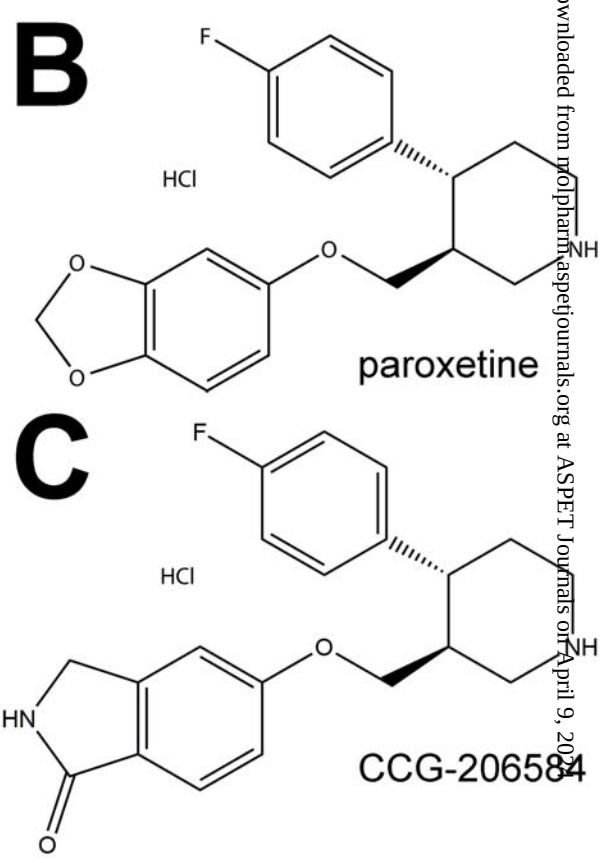

Molecular Pharmacology Fast Forward. Published on November 12, 2013 as DOI: 10.1124/mol.113.089631
This article has not been copyedited and formatted. The final version may differ from this version.

Figure 2

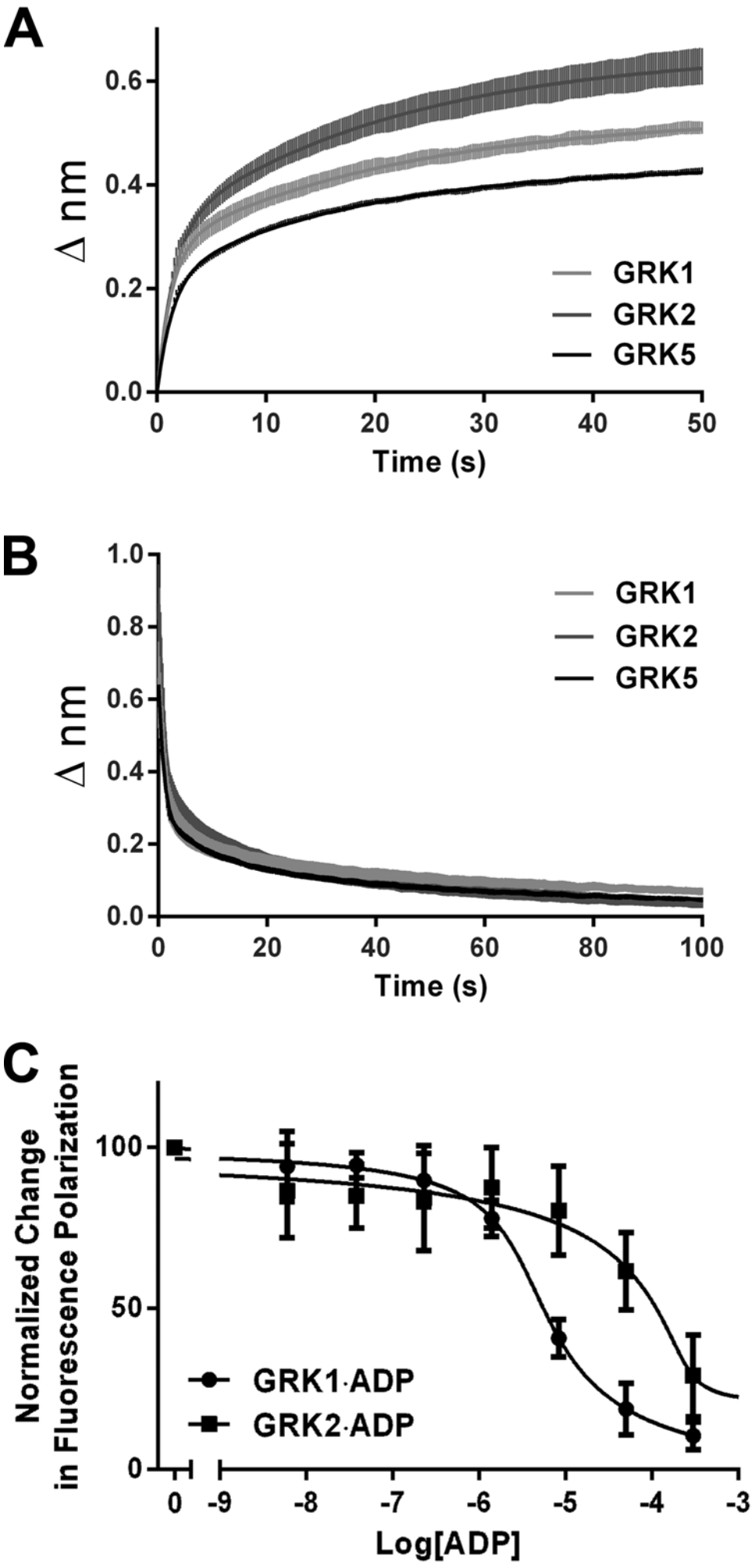

Molecular Pharmacology Fast Forward. Published on November 12, 2013 as DOI: 10.1124/mol.113.089631
This article has not been copyedited and formatted. The final version may differ from this version.

Figure 3

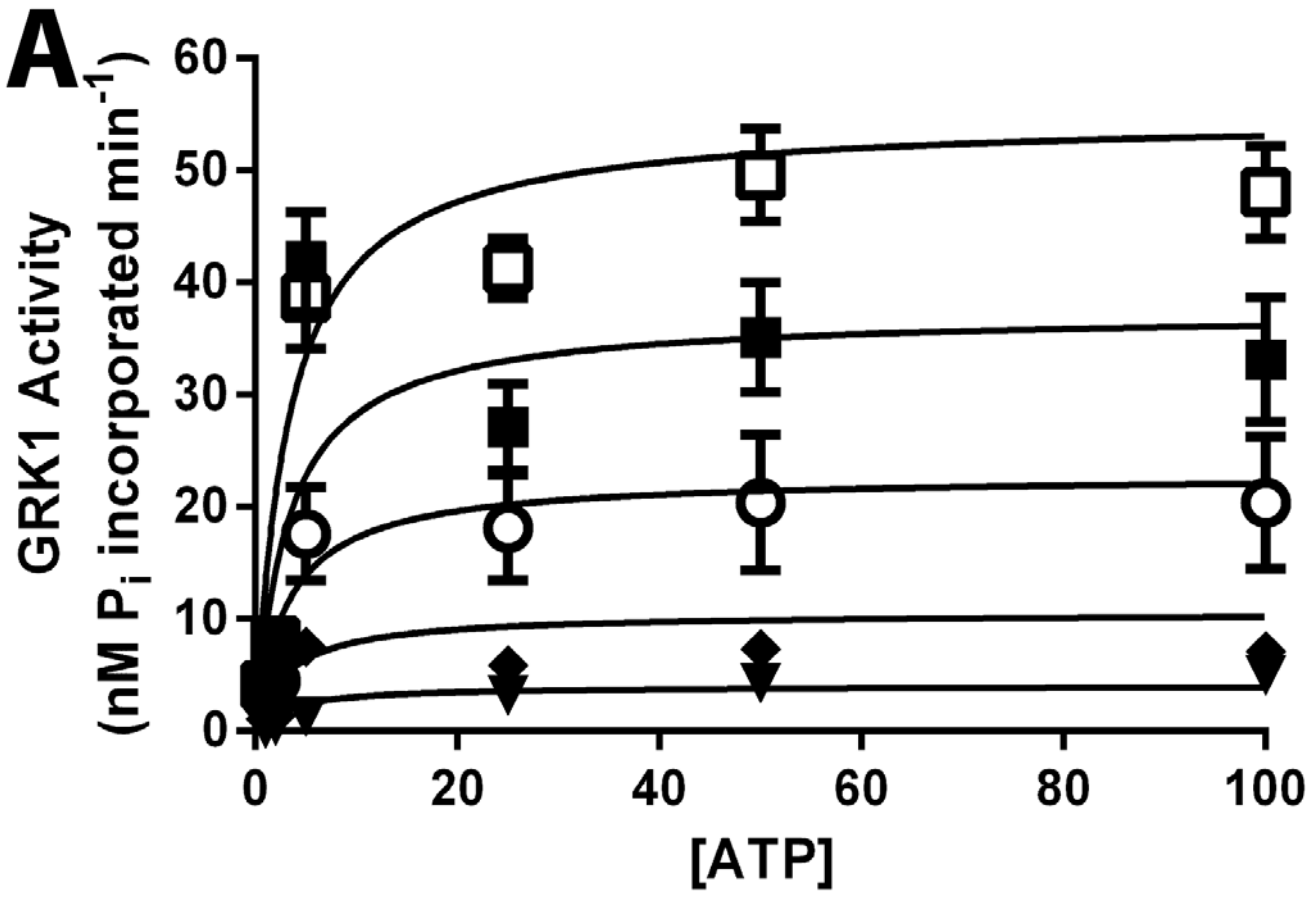

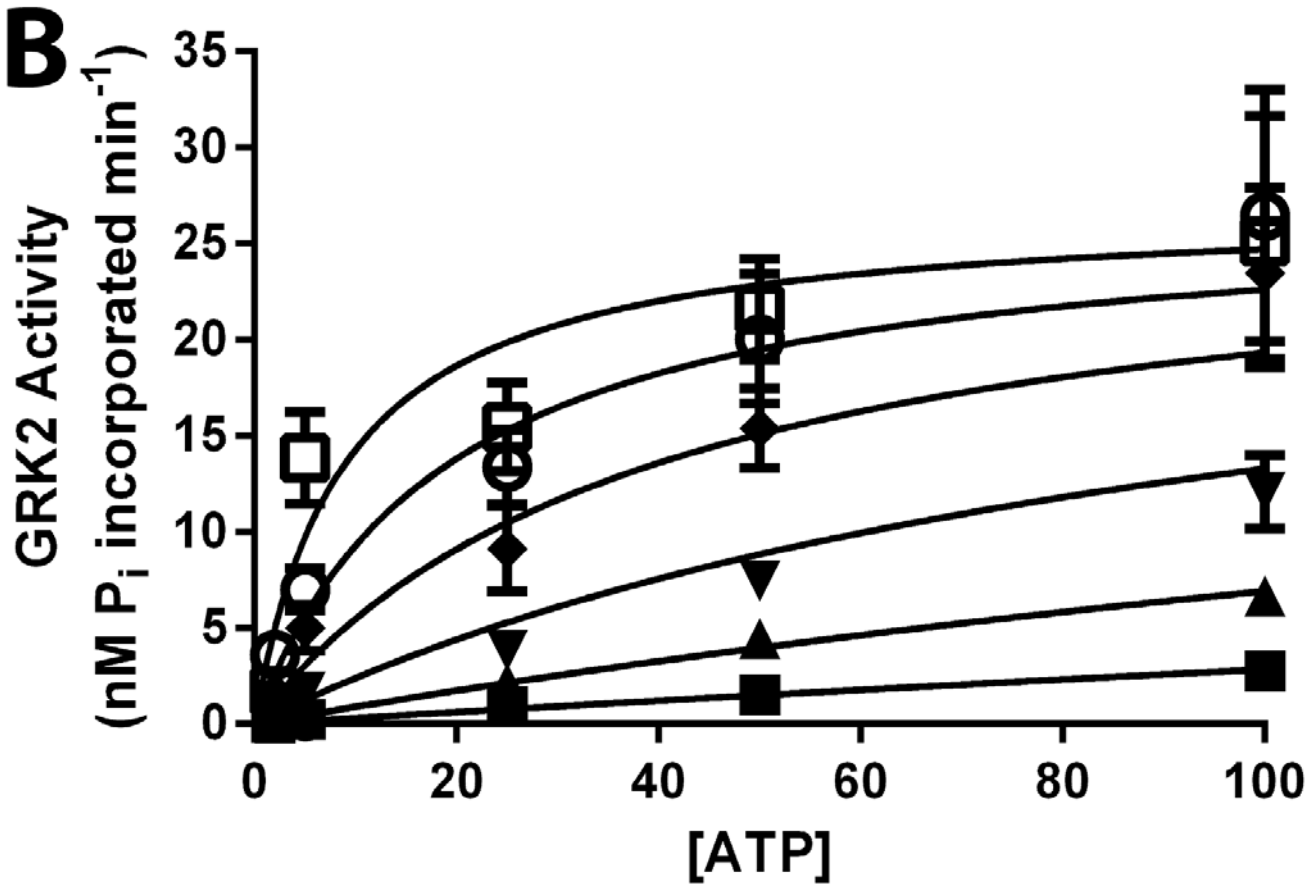

Molecular Pharmacology Fast Forward. Published on November 12, 2013 as DOI: 10.1124/mol.113.089631
This article has not been copyedited and formatted. The final version may differ from this version.

Figure 4

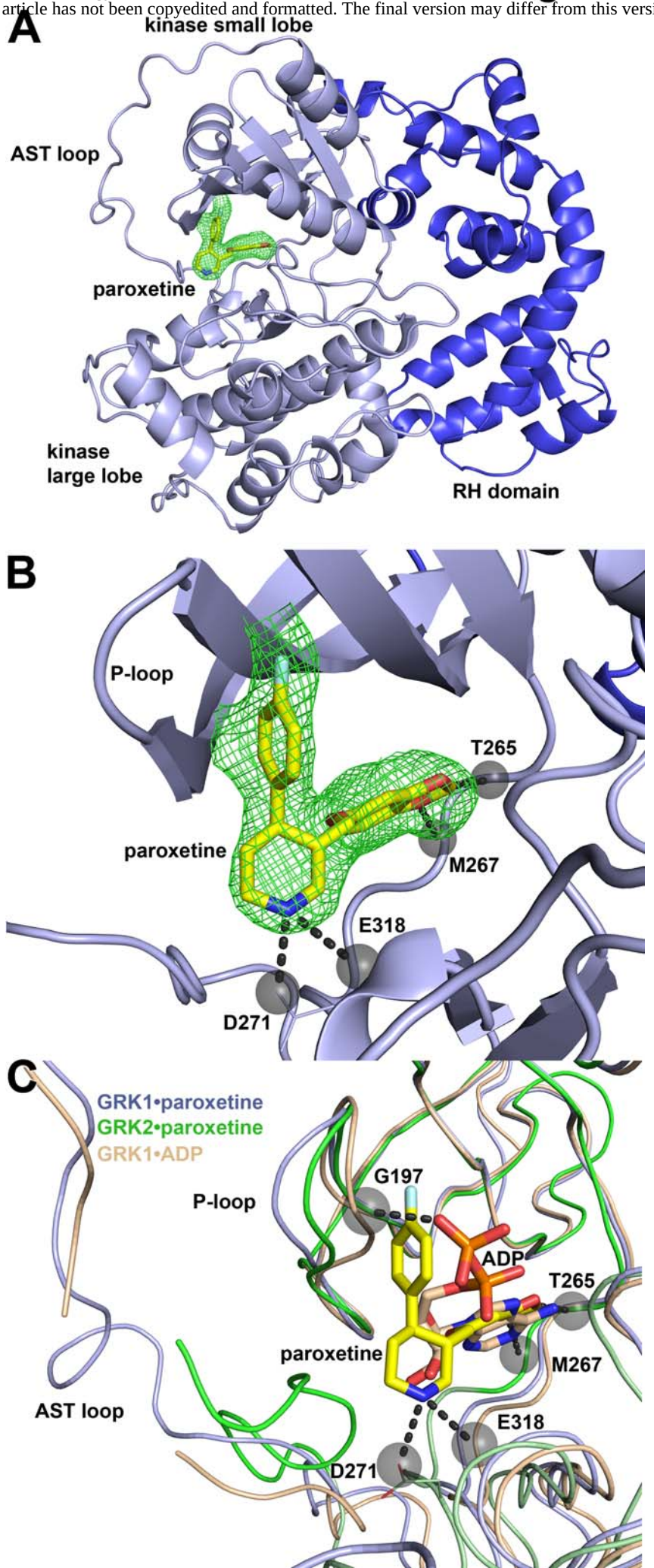

Molecular Pharmacology Fast Forward. Published on November 12, 2013 as DOI: 10.1124/mol.113.089631
This article has not been copyedited and formatted. The final version may differ from this version.

Figure 5

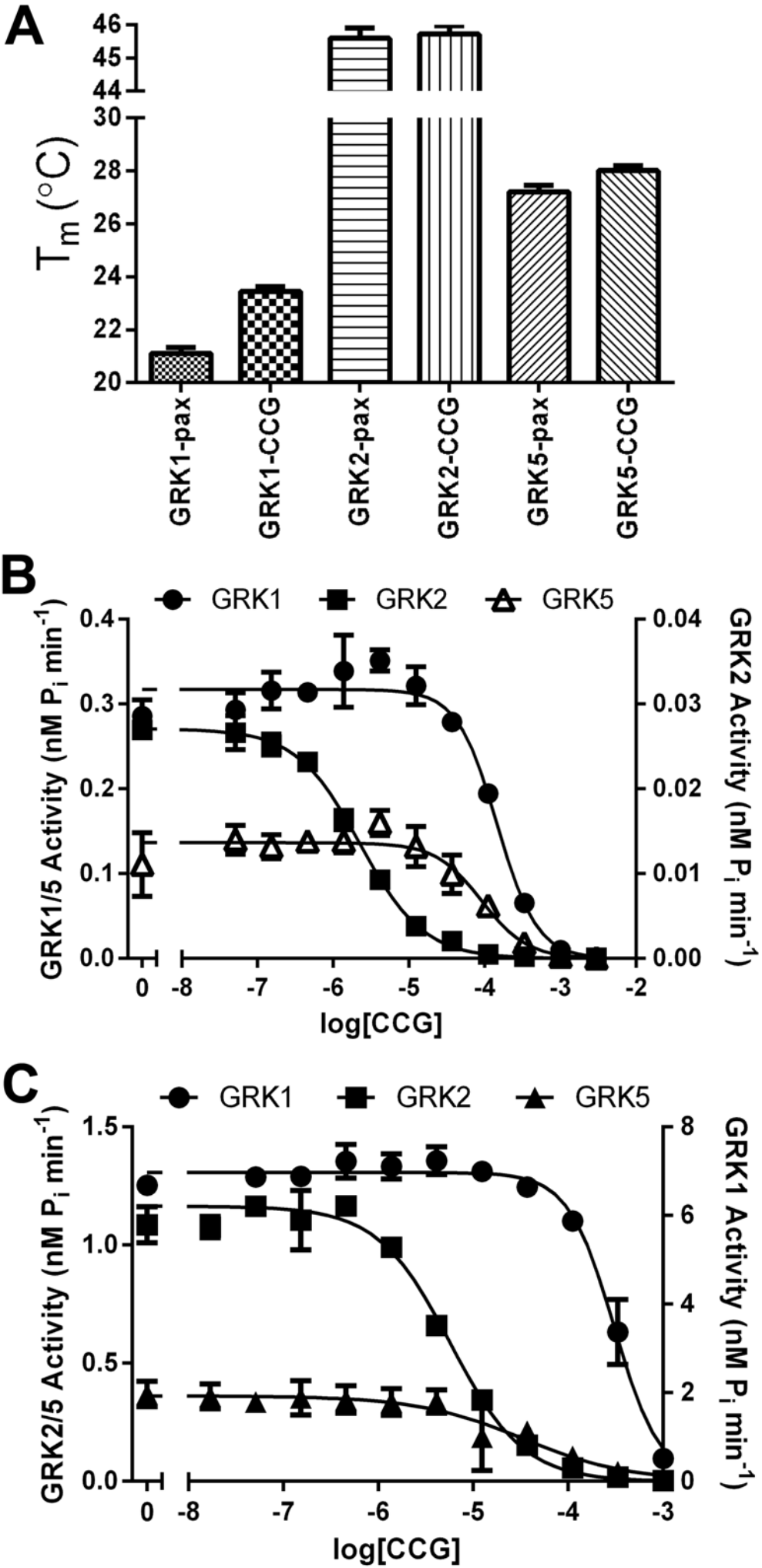

Molecular Pharmacology Fast Forward. Published on November 12, 2013 as DOI: 10.1124/mol.113.089532
This article has not been copyedited and formatted. The final version may differ from this version.

Figure 6

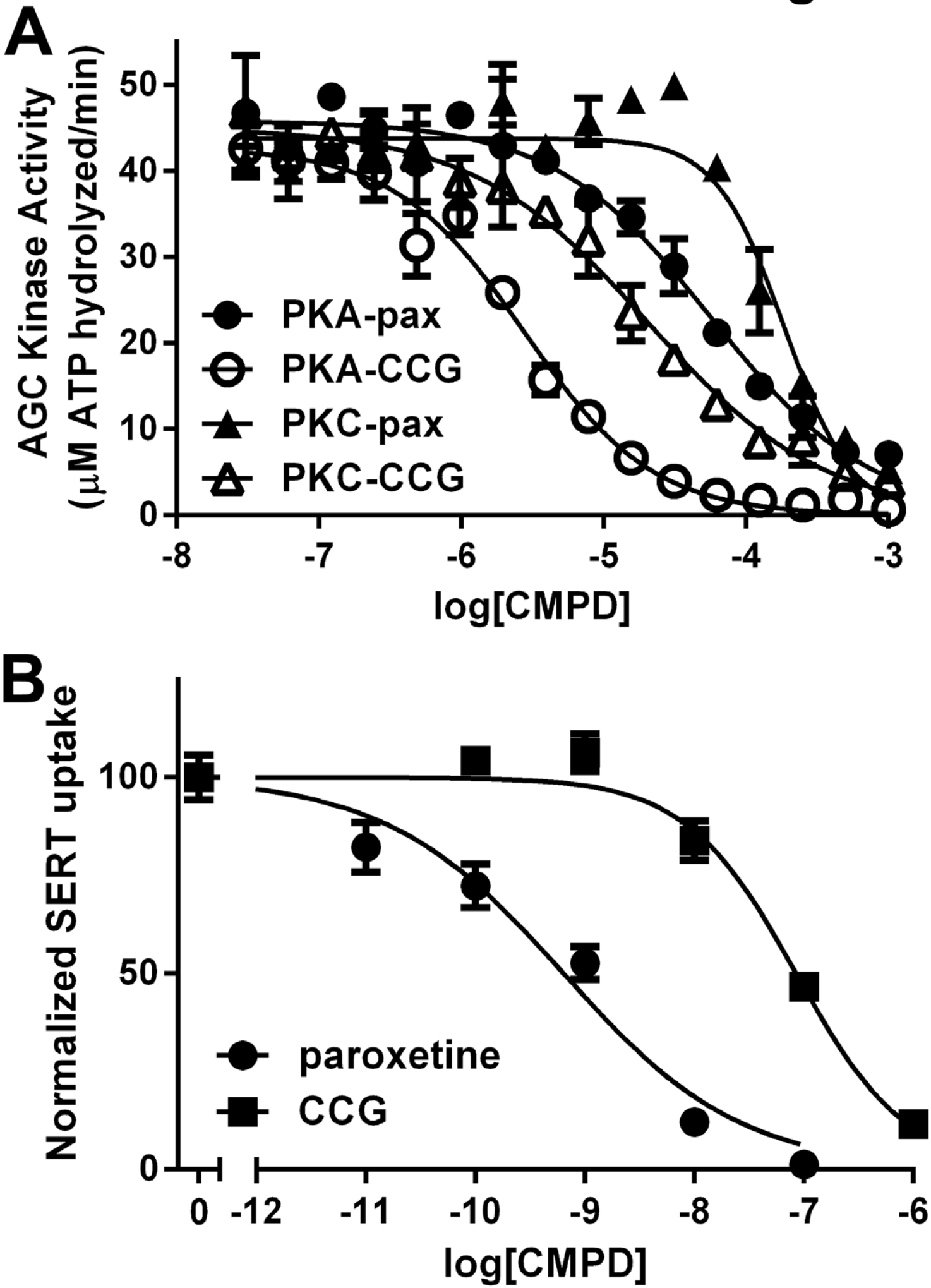

Molecular Pharmacology Fast Forward. Published on November 12, 2013 as DOI: 10.1124/mol.113.089631
This article has not been copyedited and formatted. The final version may differ from this version.

Figure 7